中国激光

基于核仁靶向碳点的双光子光动力疗法研究

雷曼[1]，逄雯[1]，石璧[2]，王晨[1]，王丹[2]，魏勋斌[3]，顾波波[1*]

[1]上海交通大学生物医学工程学院 Med-X 研究院，上海 200030；

[2]北京化工大学有机无机复合材料国家重点实验室，北京 100029；

[3]北京大学跨学部生物医学工程系，北京 100081

摘要 光动力疗法是一种利用特定波长的光激发光敏剂产生活性氧，进而杀死肿瘤细胞或者病变组织的方法。近年来，光动力疗法以其非侵入性、副作用小等优点受到了国内外的广泛关注，但该方法的应用却受到了激发光穿透深度及光敏剂亚细胞靶向能力的限制。本研究团队合成、表征了具有核仁靶向能力的碳点光敏剂，并将其用于细胞双光子光动力疗法，在低剂量的光照和光敏剂条件下，获得了优异的治疗效果。

关键词 医用光学；光动力疗法；双光子吸收；核仁靶向；碳点

中图分类号 R454.2 **文献标志码** A **DOI**：10.3788/CJL202249.1507104

1 引 言

癌症是威胁人类健康的重大疾病之一，有效的肿瘤治疗是降低死亡率的关键。目前临床使用的肿瘤治疗方法主要包括手术切除、化疗和放疗等，但这些方法都有一定的局限性，同时也存在一定的副作用[1-2]和并发症[3-4]。在众多肿瘤治疗新方法中，光动力疗法（PDT）是一种极具潜力的治疗恶性肿瘤的新技术[5-7]。光动力疗法是利用无毒性光敏剂在特定波长光照射下产生的活性氧（ROS）与癌细胞内的生物分子发生氧化反应，产生细胞毒性，进而杀伤肿瘤细胞的一种治疗方法[8-9]。光动力疗法具有治疗精准、副作用小、非侵入等优点，自 20 世纪 80 年代首次应用于临床试验以来，得到了快速发展，特别是在肿瘤学[10-12]、眼科和皮肤科等领域发展迅猛。肿瘤的光动力治疗效果不仅取决于光敏剂产生活性氧的量，还取决于光敏剂的亚细胞定位[13-14]。

近年来的研究工作主要集中于研发具有高活性氧产生效率和亚细胞结构靶向能力的光敏剂。国内外研究团队研制了诸多高性能光敏剂[15-17]，包括聚集诱导发光光敏剂、石墨烯量子点、金属-有机物框架量子点[18]、半导体纳米颗粒等[19-21]，其中石墨烯量子点的活性氧产率高达 1.3[21]。此外，靶向线粒体[22]、溶酶体[23]、内质网[24]、高尔基体[25]、核仁[26]等亚细胞靶点的光动力疗法已经得到了深入且充分的研究，其中核仁靶向的光动力疗法取得了良好的肿瘤治疗效果。

但由于能级的限制，几乎所有光敏剂的吸收波长都位于可见光波段[27]。由于可见光在生物组织中的穿透深度有限[28-29]，光动力疗法在深层肿瘤组织及肿瘤内部产生的活性氧非常有限，因此，光动力疗法在临床中主要用于浅表肿瘤的治疗[5]。但是，深层肿瘤组织的光动力治疗技术仍是基础研究和临床应用需要攻克的技术难题，迫切需要开发出适用于深层肿瘤组织光动力治疗的新技术、新方法。自 Prasad 研究团队[30]于 1997 年提出双光子光动力疗法的概念以来，国内外多个研究机构致力于该领域的研究，开展了各具特色的研究工作，并取得了一系列具有较高影响力的原创性成果[31-35]。但目前还没有关于核仁靶向的双光子光动力治疗的报道。

将具有核仁靶向能力的光敏剂用于双光子的光动力治疗，能够最大程度地发挥光动力治疗的潜能。虽然最新的研究成果已经表明核仁是一个更加有效的肿瘤治疗新靶点[36-37]，但是目前的绝大多数光敏剂并不能直接进入细胞核中，需要进行一定的修饰才能具有核仁靶向能力。最常用的修饰方法是在光敏剂表面修饰核定位信号[38-39]，如用叶酸和姜黄素对碳纳米点（简称“碳点”）进行表面修饰，利用叶酸介导的内化机制使碳点具有核仁靶向能力；此外，使用具有核仁靶向能力的纳米颗粒作为光敏剂的载体，也能使光敏剂特异性靶向到核仁[40]。但是此类光敏剂普遍存在合成过程繁琐、修饰效率低、复合颗粒不稳定等问题，因此迫切需要找到一种合成简单、无需修饰的核仁靶向光敏剂，用于双光子光动力治疗。

本研究团队以柠檬酸和乙二胺为原材料，通过简

收稿日期：2021-11-29；**修回日期**：2022-01-10；**录用日期**：2022-02-11

基金项目：国家自然科学基金（61805135）、国家重点研发计划（2019YFC1604604，2021YFF0502900）、上海市科学技术委员会项目（19DZ2280300）、上海市教委创新培育研究计划（ZXWF082101）、上海交通大学医工交叉研究基金（ZH2018QNA43）

通信作者：*bobogu@sjtu.edu.cn

单的微波加热法合成了一种具有核仁靶向能力的碳点，将其作为光敏剂，实现了高效的核仁靶向光动力治疗。此外，本研究团队表征了碳点的吸收光谱、荧光光谱和粒径，测定了碳点的双光子吸收截面、双光子激发荧光和双光子激发产生活性氧的能力，表征了碳点的细胞毒性和核仁靶向能力。随后，在 740 nm 波长飞秒激光作用下，研究了以碳点作为光敏剂的双光子光动力疗法对 HeLa 细胞的治疗效果。合成的碳点在实验中表现出了优异的性能和治疗效果，在双光子光动力治疗中具有一定的发展潜力。

2 实验材料与方法

2.1 实验材料

柠檬酸(CA)购于北京化学工业集团有限公司，乙二胺(EDA)购于福晨(天津)化学试剂有限公司，DMEM 培养基和磷酸盐缓冲生理盐水(PBS，1×)购于 HyClone 公司，胎牛血清(FBS)购于 ScienCell 公司，碘化丙啶(PI)购于 Sigma 公司，钙黄绿素-AM(Calcein-AM)购于 Biolegend 公司，细胞计数试剂盒(CCK-8)购于 Dojindo 公司，SYTO RNASelect 购于 Invitrogen 公司，HeLa(人类宫颈癌细胞系)购于 ScienCell 公司。

2.2 碳点的制备

称取 1.26 g 柠檬酸和 1.65 mL 乙二胺，将两者充分混匀后溶于 30 mL 超纯水中，再放入微波炉中用中高火加热，待观察到烧杯中的水分基本蒸干，液体变为深棕色黏稠状半固体时停止加热。将得到的产物溶于 30 mL 超纯水中，并用超声水浴锅使产物充分溶解，得到澄清的深棕色溶液。设定电热套温度为 380 ℃，将重悬后的溶液放入 50 mL 烧杯中并在预热好的电热套上加热，待观察到溶液中的水分基本被蒸干，溶液变为棕褐色黏稠状半固体时开始计时，继续加热 5 min 进行碳化。

将得到的碳化产物冷却到室温并溶于 20 mL 超纯水中，取澄清溶液置于离心管中，以 8000 r/min 的速度离心 10 min，取上清液再次进行离心，重复三次，去除溶液中的大颗粒碳化物。紧接着将上清液用孔径为 200 nm 的滤膜过滤，然后将得到的滤液转移到 3000 Da(1 Da=1 u)超滤离心管中，以 7500 r/min 的速度离心 10 min。将得到的滤液放入冻干机中冻干，得到深棕色粉末，此即为实验所需的小粒径碳点。

2.3 碳点物理性质的表征

在本研究中，使用紫外分光光度计(AuCy UV1901PC)测量碳点的吸收光谱，使用荧光光谱仪(HITACHI F2700)测量碳点的荧光光谱，使用动态光散射仪(Malvern ZETASIZER NANO)测量碳点的粒径。

2.4 CCK-8 检验碳点的生物相容性

配制含有 0，250，500，750 μg/mL 碳点的培养基溶液。将 HeLa 细胞传入 96 孔板中，待细胞贴壁后将培养基替换成含相应质量浓度碳点的培养基，分别在孵育箱中培养 24 h 和 48 h。孵育结束后用针筒吸出含碳点的培养基，并加入含 10% CCK-8 的培养基，放入孵育箱中反应 1 h。用酶标仪(SpectraMax i3X)检测溶液在 450 nm 处的吸光度，以此表征材料的生物相容性。

2.5 碳点的双光子激发

750 nm 飞秒激光通过物镜(16×)会聚后用于激发碳点溶液。用相机记录碳点的荧光发光情况，以衡量碳点的双光子吸收能力。

2.6 碳点核仁靶向能力检验

选用商用核仁染料 SYTO RNASelect 与碳点共染 HeLa 细胞，通过荧光显微成像验证碳点的核仁靶向能力。在实验过程中，通过设定不同的激发光波长和接收波段来区分碳点和 SYTO RNASelect 的荧光，其中：SYTO RNASelect 的激发波长为 488 nm，荧光接收范围为 510～540 nm；碳点的激发波长为 552 nm，荧光接收范围为 560～590 nm。

2.7 碳点的活性氧产生能力

选用商用活性氧指示剂 9，10-Anthracenediyl-bis(methylene)-dimalonic acid (ABDA)来表征碳点的活性氧产量，其检测原理是：活性氧可以消耗 ABDA，使其紫外-可见光吸收光谱的特征吸收峰强度下降。通过测量 ABDA 特征吸收峰的变化来表征碳点的活性氧产生能力。

在本实验中，首先将 ABDA 粉末溶于二甲基亚砜(DMSO)，配制成浓度为 5 mmol/L 的母液，然后用超纯水将碳点粉末配制成 4 mg/mL 的溶液。将 1967.5 μL 超纯水、20 μL ABDA 母液以及 12.5 μL 碳点溶液均匀混合，得到待测溶液。使用功率密度为 100 mW/cm^2 的白光激发待测溶液，并在照射不同时间后，使用紫外-可见光分光光度计测量混合溶液的吸收光谱。

2.8 HeLa 细胞的光动力治疗

用分析天平称取 4 mg 碳点，将称量好的碳点加入 1 mL 超纯水中配制成 4 mg/mL 碳点水溶液；用旋涡仪使碳点完全溶解，得到澄清的深棕色水溶液；用 DMEM 培养基稀释碳点水溶液至 500 μg/mL，避光存放备用。

待共聚焦小皿中的 HeLa 细胞贴壁后，将培养基更换为含碳点的培养基，然后放在孵育箱中孵育 3 h(37 ℃，5% CO_2)，用于细胞光动力治疗研究。使用飞秒激光(740 nm，28 mW)对细胞进行不同治疗时间的光动力治疗。治疗结束后，将共聚焦小皿放回孵育箱中孵育 4 h，之后采用荧光成像方法评估细胞双光子光动力疗法的效果。

2.9 Calcein-AM/PI 活死细胞染色

同时取 PI 和 Calcein-AM 各 4 μL，用培养基配制浓度为 2 μmol/L 的染液。Calcein-AM 可以穿过细胞膜进入细胞内，活细胞中的酯酶会脱去它的 AM 基团，产生 Calcein，即钙黄绿素。钙黄绿素可以发出很强的绿色荧光，因此，活细胞在共聚焦显微镜下呈现绿色。PI 不能穿过活细胞的细胞膜，但能通过死细胞受损的细胞膜进入胞内，并嵌入到细胞的 DNA 中。PI 与 DNA 嵌合后

会发出红色荧光，使死细胞在共聚焦显微镜下呈现红色。因此，选用 PI 和 Calcein-AM 共染细胞分别标定死细胞和活细胞，进而评估双光子光动力疗法的效果。

双光子光动力治疗 4 h 后，将 PI/ Calcein-AM 的混合染液与治疗后的 HeLa 细胞共孵育 30 min；之后使用 PBS 清洗细胞两次，去除残留的 PI 和 Calcein-AM，加入 2 mL 普通培养基，用于细胞成像。其中：Calcein-AM 通道（活细胞通道）的激发波长为 488 nm，荧光接收范围为 510～540 nm；PI 通道（死细胞通道）的激发波长为 552 nm，荧光接收范围为 560～590 nm。

2.10 光动力治疗系统

如图 1 所示，本研究团队基于奥林巴斯显微系统（OLYMPUS FLUOVIEW FVMPE-RS）和飞秒激光器（Coherent Ultra II），搭建了用于光动力治疗的光学系统。

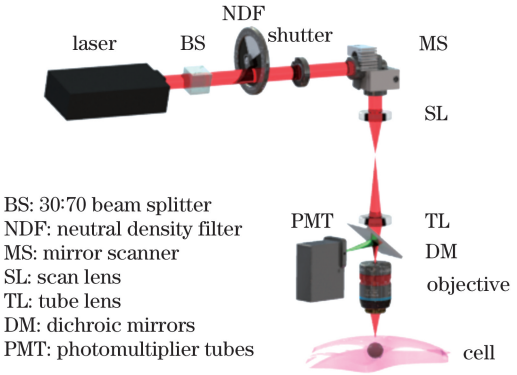

图 1 光动力治疗系统示意图

Fig. 1 Schematic of optical system for photodynamic therapy

3 分析与讨论

3.1 碳点的合成及表征

碳点是一种新兴的纳米材料，相比于量子点，碳点具有更好的生物安全性和快速代谢特性，已被广泛应用于生物医学光学成像和治疗中[41]。本研究团队选用柠檬酸和乙二胺作为原材料，通过微波加热法合成碳点。通过动态光散射（DLS）方法测得合成碳点的粒径为 0.649 nm±0.124 nm，如图 2(a)所示，较小的粒径有助于快速代谢。合成的碳点具有宽带吸收（300～

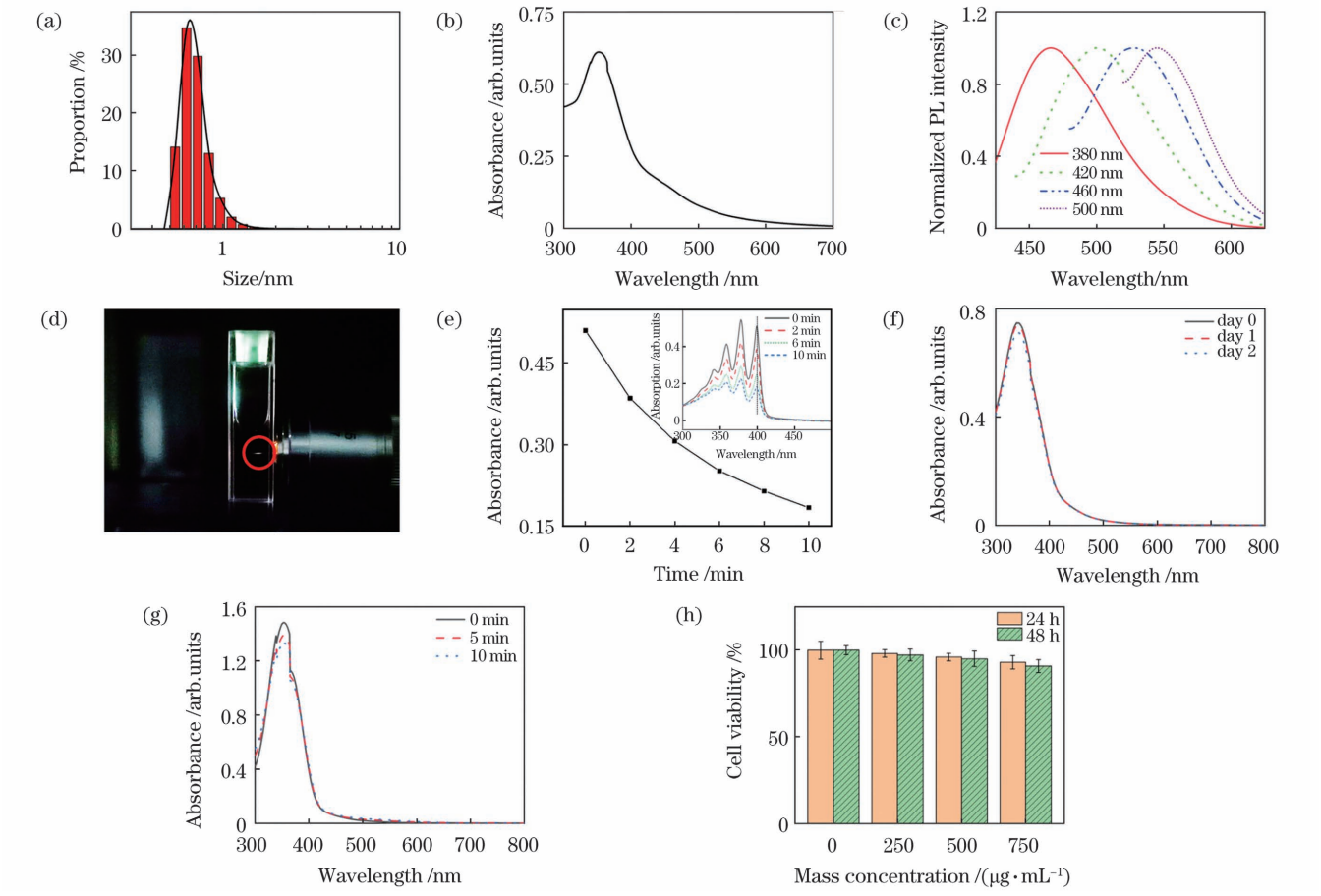

图 2 碳点的性能表征。(a)粒径；(b)吸收光谱；(c)荧光光谱；(d)双光子激发荧光；(e)ABDA 特征吸收峰（λ=399 nm）强度随光照时间的变化曲线，插图是碳点和 ABDA 混合溶液在不同时间光照下的紫外-可见光吸收光谱；(f)在 PBS 中放置不同时间后碳点的吸收光谱；(g)不同光照时间下碳点的吸收光谱；(h)生物相容性评估

Fig. 2 Characterization of C-dots. (a) Particle size; (b) absorption spectrum; (c) fluorescence spectra; (d) two-photon excited fluorescence; (e) variation curve of characteristic absorption peak (λ=399 nm) of ABDA under light irradiation with different light irradiation time, where the inset shows UV-Vis spectra of ABDA and C-dots under light irradiation for different time; (f) absorption spectra of C-dots in PBS for different time; (g) absorption spectra of C-dots under light irradiation for different time; (h) assessment of biocompatibility of C-dots

700 nm)，其主吸收峰和肩吸收峰分别位于 360 nm 和 450 nm 处，如图 2(b)所示。同时，合成碳点的荧光具有激发波长依赖性，如图 2(c)所示，该特性是碳基荧光材料的特征之一。最新的研究表明，碳点的双光子吸收截面高达 16000 GM±1500 GM[42]，这使得其可以成为理想的双光子探针。如图 2(d)所示，飞秒激光(750 nm，45 mW)可以有效激发碳点的双光子荧光信号。选用 ABDA 作为活性氧指示剂，使用白光(100 mW/cm^2)激发碳点，研究其活性氧产生能力。如图 2(e)所示，在白光照射 10 min 内，ABDA 的特征吸收峰强度迅速下降。这是因为溶液中的 ABDA 被碳点产生的活性氧快速消耗，说明碳点具有优异的活性氧产生能力。将碳点溶于 PBS 溶液中，通过测量其吸收光谱的变化来研究其在生物环境内的稳定性。如图 2(f)所示，在 48 h 内，吸收光谱没有显著变化，证明碳点具有良好的生物稳定性，可以应用于生物医学研究。抗光漂白能力决定了碳点在生物成像和治疗中的性能，是光敏剂的重要特性。使用白光(100 mW/cm^2)连续激发碳点，并通过测量其吸收光谱来研究其抗光漂白能力。如图 2(g)所示，经过 10 min 的连续照射，碳点的吸收光谱曲线没有明显下降，从而可以推断出碳点具有良好的抗光漂白能力。在开展生物医学应用前，用 CCK-8 试剂盒评估了碳点的生物相容性，结果如图 2(h)所示。在碳点质量浓度范围为 250～750 μg/mL，孵育时间为 24 h 或 48 h 的条件下，碳点孵育的 HeLa 细胞的活性相比于对照组均没有显著变化，说明合成的碳点具有良好的生物相容性。

3.2 碳点的核仁靶向能力研究

为了研究碳点在细胞内的定位情况，将碳点(500 μg/mL)与 HeLa 细胞共孵育 3 h 后进行荧光成像。如图 3 所示，在一些圆形区域即核仁位置可以观测到碳点的荧光信号。为了进一步确认碳点在细胞内的定位，选用商用核仁成像探针 SYTO RNASelect 和碳点共同标记 HeLa 细胞。如图 3 所示，碳点的荧光信号与 SYTO RNASelect 的荧光信号完全重叠，这表明碳点具有核仁靶向能力，可以有效标记核仁。本团队在前期关于碳点的核仁靶向机制研究[26]中，分别水解了细胞的 DNA 和 RNA，并观察了碳点的富集情况。结果显示，碳点通过与核仁中的 RNA 相互作用实现在核仁中的富集。碳点和 RNA 都具有负电性，因此，碳点与 RNA 的相互作用，即核仁的靶向能力，可以归功于碳点特殊的表面化学特性。

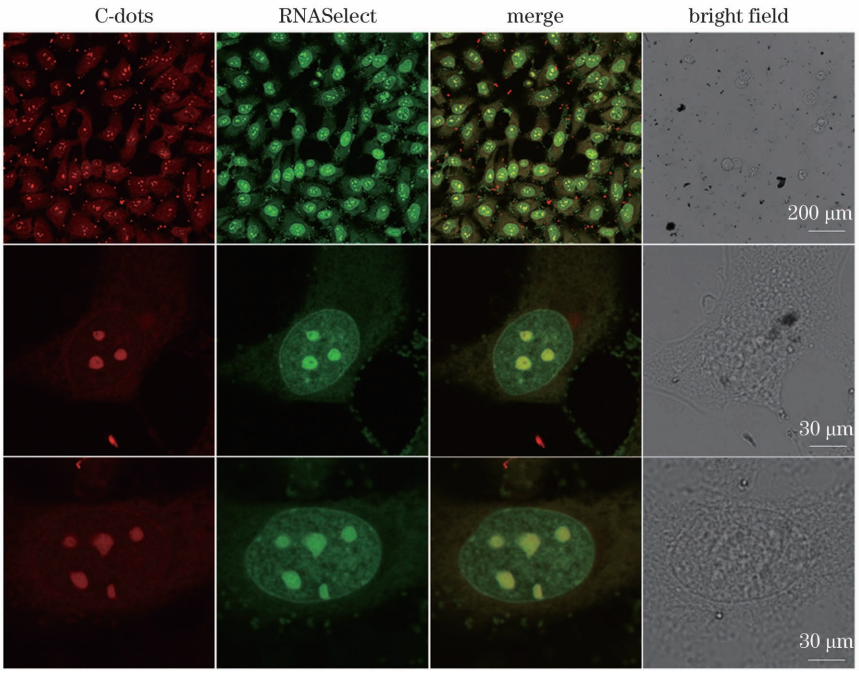

图 3 碳点与 RNASelect 共染 HeLa 细胞的荧光图像、叠加图像及明场图像，其中碳点通道的激发波长 λ_{ex}=552 nm，发射波长 λ_{em}=560～590 nm，RNASelect 通道的激发波长 λ_{ex}=488 nm，发射波长 λ_{em}=510～540 nm，RNASelect 的浓度为 10 μmol/L，碳点的质量浓度为 500 μg/mL

Fig. 3 Fluorescence images, merged images, and bright field images of HeLa cells stained with both RNASelect and C-dots, where excitation and emission wavelengths of C-dots channel are λ_{ex}=552 nm and λ_{em}=560–590 nm, excitation and emission wavelengths of RNASelect channel are λ_{ex}=488 nm and λ_{em}=510–540 nm, the concentration of RNASelect is 10 μmol/L, and the mass concentration of C-dots is 500 μg/mL

3.3 细胞的光动力治疗

为了分析碳点的细胞光动力治疗效率，将 HeLa 细胞与碳点(500 μg/mL)共孵育 3 h，之后利用飞秒激光(740 nm，28 mW)对碳点标记的 HeLa 细胞进行光照。进行不同时间的光照后，选用 Calcein-AM 和 PI 对治疗后的 HeLa 细胞染色，并通过荧光成像方法评

估治疗效果。如图 4 所示，在飞秒激光扫描区域，随着扫描时间延长，更多的细胞呈 PI 阳性，即坏死。当扫描时间为 45 s 时，几乎所有的细胞都坏死。可以推测，核仁靶向光动力疗法通过原位产生的活性氧破坏癌细胞的核仁 RNA，从而实现优异的抗肿瘤效果。飞秒激光扫描区域外都显示 Calcein 绿色荧光，再次证明了碳点良好的生物相容性。同时，仅用飞秒激光扫描（740 nm，28 mW，3 min）的 HeLa 细胞也显示 Calcein 绿色荧光，从而排除了飞秒激光扫描对治疗效果的影响。相比于近年来发展的双光子光动力疗法（如表 1 所示），本实验中使用的光剂量更低且更具有优势。

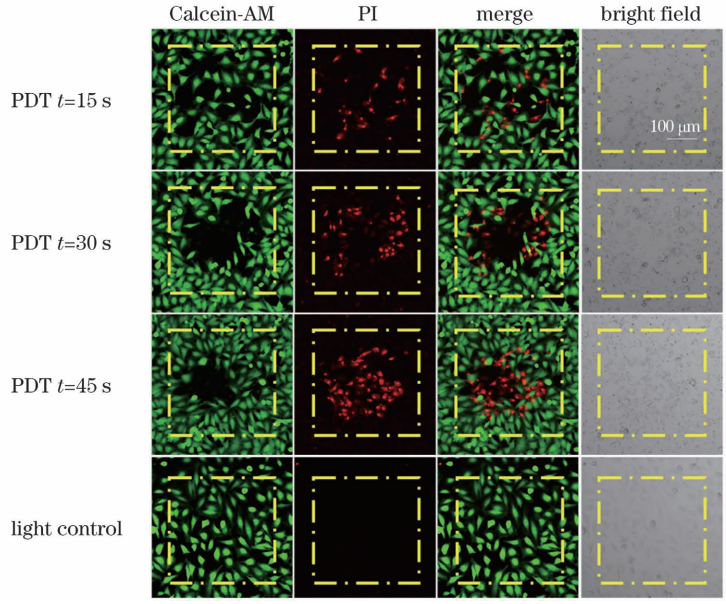

图 4 核仁靶向双光子光动力疗法引起细胞坏死。孵育/未孵育碳点的 HeLa 细胞分别受到不同时间的双光子扫描，其中 Calcein 通道的激发波长 λ_{ex} = 488 nm，发射波长 λ_{em} = 505～525 nm，PI 通道的激发波长 λ_{ex} = 532 nm，发射波长 λ_{em} = 605～625 nm，黄色方块表示扫描区域

Fig. 4 Necrosis development in response to nucleolus-targeted two-photon PDT. HeLa cells incubated with/without C-dots were irradiated by two-photon scans with different time, where excitation and emission wavelengths of Calcein channel are λ_{ex}=488 nm and λ_{em}=505–525 nm, excitation and emission wavelengths of propidium iodide (PI) channel are λ_{ex}=532 nm and λ_{em}=605–625 nm, and scanned areas are indicated by yellow squares

表 1 双光子光动力治疗中的光剂量

Table 1 Light dose for two-photon photodynamic therapy

Cell	Photosensitizer	Photosensitizer concentration	Excitation wavelength /nm	Luminous flux density	Excitation time	Light dose /(J·cm^{-2})	Ref.
HepG2	AuNC	100 μg·mL^{-1}	800	13.8 W·cm^{-2}	5 min	4140	[43]
HeLa	T-TPEDC	10 μg·mL^{-1}	800	60 J·cm^{-2} per scan	120 scans	7200	[31]
A549	DPASP	50 μmol·L^{-1}	960	1.5 W/cm^{2}	10 min	900	[44]
HeLa	TQ-BTPE	2 μmol·L^{-1}	850	40 J·cm^{-2} per scan	60 scans	2400	[45]
HeLa	RTCD	100 μg·mL^{-1}	638	1 W·cm^{-2}	5 min	300	[46]
HeLa	AuNP	40 pmol·L^{-1}	808	3 W·cm^{-2}	15 min	2700	[15]
HeLa	CNDs	500 μg·mL^{-1}	740	3.57 W·cm^{-2}	45 s	160.65	This work

4 结 论

本研究团队设计并合成了具有核仁靶向和活性氧产生能力的新型碳点。核仁是一个更加有效的肿瘤治疗新靶点，本研究团队合成的碳点具有靶向核仁能力，可以在癌细胞核仁处产生活性氧，从而在低剂量的光照和光敏剂条件下，实现有效的肿瘤细胞双光子光动力治疗。合成的碳点具有良好的生物相容性和快速代谢等优势，并且双光子激发可以获得更大的穿透深度。因此，基于碳点的核仁靶向双光子光动力疗法在未来的转化医学研究中具有巨大潜力。

参 考 文 献

[1] Carelle N, Piotto E, Bellanger A, et al. Changing patient perceptions of the side effects of cancer chemotherapy[J]. Cancer, 2002, 95(1): 155-163.

[2] Browning R J, Reardon P J T, Parhizkar M, et al. Drug

delivery strategies for platinum-based chemotherapy[J]. ACS Nano, 2017, 11(9): 8560-8578.

[3] Bruheim K, Guren M G, Skovlund E, et al. Late side effects and quality of life after radiotherapy for rectal cancer[J]. International Journal of Radiation Oncology Biology Physics, 2010, 76(4): 1005-1011.

[4] Chang-Claude J, Popanda O, Tan X L, et al. Association between polymorphisms in the DNA repair genes, XRCC1, APE1, and XPD and acute side effects of radiotherapy in breast cancer patients[J]. Clinical Cancer Research: an Official Journal of the American Association for Cancer Research, 2005, 11(13): 4802-4809.

[5] Dolmans D E J G J, Fukumura D, Jain R K. Photodynamic therapy for cancer[J]. Nature Reviews Cancer, 2003, 3(5): 380-387.

[6] Castano A P, Mroz P, Hamblin M R. Photodynamic therapy and anti-tumour immunity[J]. Nature Reviews Cancer, 2006, 6(7): 535-545.

[7] 黄燕霞, 许皓, 栾萍, 等. β-淀粉样蛋白斑块的无标记成像及光动力降解[J]. 中国激光, 2020, 47(2): 0207029.
Huang Y X, Xu H, Luan P, et al. Label-free imaging of β-amyloid plaques and photodynamic degradation[J]. Chinese Journal of Lasers, 2020, 47(2): 0207029.

[8] MacDonald I J, Dougherty T J. Basic principles of photodynamic therapy[J]. Journal of Porphyrins and Phthalocyanines, 2001, 5(2): 105-129.

[9] Alfadda A A, Sallam R M. Reactive oxygen species in health and disease[J]. Journal of Biomedicine & Biotechnology, 2012, 2012: 936486.

[10] Railkar R, Agarwal P K. Photodynamic therapy in the treatment of bladder cancer: past challenges and current innovations[J]. European Urology Focus, 2018, 4(4): 509-511.

[11] Usuda J, Kato H, Okunaka T, et al. Photodynamic therapy (PDT) for lung cancers[J]. Journal of Thoracic Oncology, 2006, 1(5): 489-493.

[12] Agostinis P, Berg K, Cengel K A, et al. Photodynamic therapy of cancer: an update[J]. CA: a Cancer Journal for Clinicians, 2011, 61(4): 250-281.

[13] de Freitas L F, Hamblin M R. Antimicrobial photoinactivation with functionalized fullerenes[M]// Grumezescu A M. Nanobiomaterials in antimicrobial therapy. Amsterdam: Elsevier, 2016: 1-27.

[14] Skovsen E, Snyder J W, Lambert J D C, et al. Lifetime and diffusion of singlet oxygen in a cell[J]. The Journal of Physical Chemistry B, 2005, 109(18): 8570-8573.

[15] Lin L Y, Pang W, Jiang X Y, et al. Light amplified oxidative stress in tumor microenvironment by carbonized hemin nanoparticles for boosting photodynamic anticancer therapy[J]. Light: Science & Applications, 2022, 11(47): 1-16.

[16] Zhou Z J, Song J B, Nie L M, et al. Reactive oxygen species generating systems meeting challenges of photodynamic cancer therapy[J]. Chemical Society Reviews, 2016, 45(23): 6597-6626.

[17] 谢丽娜, 高诚宜, 汪琪, 等. 基于切伦科夫辐射的光动力疗法用于肿瘤治疗的研究进展[J]. 激光与光电子学进展, 2020, 57(19): 190002.
Xie L N, Gao C Y, Wang Q, et al. Research progress of photodynamic therapy based on Cherenkov radiation for tumors[J]. Laser & Optoelectronics Progress, 2020, 57(19): 190002.

[18] 李阳, 王秀翊, 李艳艳, 等. 金属有机框架载药平台光动力消融乳腺癌细胞[J]. 激光与光电子学进展, 2021, 58(14): 1417002.
Li Y, Wang X H, Li Y Y, et al. Drug-loaded platform based on metal-organic framework for photodynamic ablation of breast cancer cells[J]. Laser & Optoelectronics Progress, 2021, 58(14): 1417002.

[19] Wu W, Mao D, Hu F, et al. A highly efficient and photostable photosensitizer with near-infrared aggregation-induced emission for image-guided photodynamic anticancer therapy[J]. Advanced Materials, 2017, 29(33): 1700548.

[20] Zhu H J, Li J C, Qi X Y, et al. Oxygenic hybrid semiconducting nanoparticles for enhanced photodynamic therapy[J]. Nano Letters, 2018, 18(1): 586-594.

[21] Ge J, Lan M, Zhou B, et al. A graphene quantum dot photodynamic therapy agent with high singlet oxygen generation[J]. Nature Communications, 2014, 5: 4596.

[22] Lü W, Zhang Z, Zhang K Y, et al. A mitochondria-targeted photosensitizer showing improved photodynamic therapy effects under hypoxia[J]. Angewandte Chemie (International Ed. in English), 2016, 55(34): 9947-9951.

[23] Zhang D Y, Zheng Y, Zhang H, et al. Ruthenium complex-modified carbon nanodots for lysosome-targeted one- and two-photon imaging and photodynamic therapy[J]. Nanoscale, 2017, 9(47): 18966-18976.

[24] Li W, Yang J, Luo L, et al. Targeting photodynamic and photothermal therapy to the endoplasmic reticulum enhances immunogenic cancer cell death[J]. Nature Communications, 2019, 10: 3349.

[25] Tan W Y, Zhang Q X, Wang J Q, et al. Enzymatic assemblies of thiophosphopeptides instantly target Golgi apparatus and selectively kill cancer cells[J]. Angewandte Chemie (International Ed. in English), 2021, 60(23): 12796-12801.

[26] Pang W, Jiang P F, Ding S H, et al. Nucleolus-targeted photodynamic anticancer therapy using renal-clearable carbon dots[J]. Advanced Healthcare Materials, 2020, 9(16): e2000607.

[27] DeRosa M C, Crutchley R J. Photosensitized singlet oxygen and its applications[J]. Coordination Chemistry Reviews, 2002, 233/234: 351-371.

[28] Gu B B, Yong K T, Liu B. Strategies to overcome the limitations of AIEgens in biomedical applications[J]. Small Methods, 2018, 2(9): 1700392.

[29] 林立, 李步洪. 发光二极管在光动力疗法中的应用进展[J]. 激光与光电子学进展, 2020, 57(15): 150001.
Lin L, Li B H. Application progress of light-emitting diode for photodynamic therapy[J]. Laser & Optoelectronics Progress, 2020, 57(15): 150001.

[30] Bhawalkar J D, Kumar N D, Zhao C F, et al. Two-photon photodynamic therapy[J]. Journal of Clinical Laser Medicine & Surgery, 1997, 15(5): 201-204.

[31] Gu B, Wu W, Xu G, et al. Precise two-photon photodynamic therapy using an efficient photosensitizer with aggregation-induced emission characteristics[J]. Advanced Materials, 2017, 29(28): 1701076.

[32] Huang H Y, Yu B L, Zhang P Y, et al. Highly charged ruthenium(II) polypyridyl complexes as lysosome-localized photosensitizers for two-photon photodynamic therapy[J]. Angewandte Chemie (International Ed. in English), 2015, 54(47): 14049-14052.

[33] Collins H A, Khurana M, Moriyama E H, et al. Blood-vessel closure using photosensitizers engineered for two-photon excitation[J]. Nature Photonics, 2008, 2(7): 420-424.

[34] Gary-Bobo M, Mir Y, Rouxel C, et al. Mannose-functionalized mesoporous silica nanoparticles for efficient two-photon photodynamic therapy of solid tumors[J]. Angewandte Chemie (International Ed. in English), 2011, 50(48): 11425-11429.

[35] Zou Q L, Zhao H Y, Zhao Y X, et al. Effective two-photon excited photodynamic therapy of xenograft tumors sensitized by water-soluble bis(arylidene)cycloalkanone photosensitizers[J]. Journal of Medicinal Chemistry, 2015, 58(20): 7949-7958.

[36] Mijatovic T, de Nève N, Gailly P, et al. Nucleolus and c-Myc: potential targets of cardenolide-mediated antitumor activity[J]. Molecular Cancer Therapeutics, 2008, 7(5): 1285-1296.

[37] Hua X W, Bao Y W, Wu F G. Fluorescent carbon quantum dots with intrinsic nucleolus-targeting capability for nucleolus imaging and enhanced cytosolic and nuclear drug delivery[J]. ACS

Applied Materials & Interfaces, 2018, 10(13): 10664-10677.
[38] Tian X H, Zhu Y Z, Zhang M Z, et al. Localization matters: a nuclear targeting two-photon absorption iridium complex in photodynamic therapy[J]. Chemical Communications, 2017, 53(23): 3303-3306.
[39] Nasrin A, Hassan M, Gomes V G. Two-photon active nucleus-targeting carbon dots: enhanced ROS generation and photodynamic therapy for oral cancer[J]. Nanoscale, 2020, 12(40): 20598-20603.
[40] Pan L M, Liu J N, Shi J L. Cancer cell nucleus-targeting nanocomposites for advanced tumor therapeutics[J]. Chemical Society Reviews, 2018, 47(18): 6930-6946.
[41] Panwar N, Soehartono A M, Chan K K, et al. Nanocarbons for biology and medicine: sensing, imaging, and drug delivery[J]. Chemical Reviews, 2019, 119(16): 9559-9656.
[42] Tong G S, Wang J X, Wang R B, et al. Amorphous carbon dots with high two-photon fluorescence for cellular imaging passivated by hyperbranched poly(amino amine)[J]. Journal of Materials Chemistry B, 2015, 3(4): 700-706.
[43] Han R C, Zhao M, Wang Z W, et al. Super-efficient *in vivo* two-photon photodynamic therapy with a gold nanocluster as a type I photosensitizer[J]. ACS Nano, 2020, 14(8): 9532-9544.
[44] He X J, Bo S T, Gao M, et al. Stereotactic photodynamic therapy using a two-photon AIE photosensitizer[J]. Small, 2019, 15(50): e1905080.
[45] Wang S W, Chen H, Liu J, et al. NIR-II light activated photosensitizer with aggregation-induced emission for precise and efficient two-photon photodynamic cancer cell ablation[J]. Advanced Functional Materials, 2020, 30(30): 2002546.
[46] Lesani P, Mohamad Hadi A H, Lu Z, et al. Design principles and biological applications of red-emissive two-photon carbon dots[J]. Communications Materials, 2021, 2: 108.

Two-Photon Photodynamic Therapy Using Nucleolus-Targeted Carbon Dots

Lei Man[1], Pang Wen[1], Shi Bo[2], Wang Chen[1], Wang Dan[2], Wei Xunbin[3], Gu Bobo[1*]
[1] *Med-X Research Institute and School of Biomedical Engineering, Shanghai Jiao Tong University, Shanghai* 200030, *China*;
[2] *State Key Laboratory of Organic-Inorganic Composites, Beijing University of Chemical Technology, Beijing* 100029, *China*;
[3] *Biomedical Engineering Department, Peking University, Beijing* 100081, *China*

Abstract

Objective Photodynamic therapy (PDT), which canablate cancer cells or diseased tissue by the generated reactive oxygen species (ROS) once the photosensitizers (PSs) are excited by light with specific wavelength, has attracted various attention in the last decades due to its unique advantages, including non-invasiveness, few side-effects, etc. The advancement of PDT has been significantly restricted by the penetration depth of the excitation light and sub-cellular organelles targeting capability. Here, an effective carbon dots (C-dots) photosensitizer with intrinsic nucleolus-targeting capability is synthesized, characterized, and employed for *in vitro* photodynamic anticancer therapy with enhanced treatment performance at a low dose of PS and light irradiation.

Methods The optical system, which included a microscope and femtosecond laser, was designed for two-photon phototherapy. The nucleolus-targeted C-dots were synthesized using microwave heating. The characteristics of synthesized C-dots including particles size, absorption and emission, two-photon fluorescence, photobleaching, biocompatibility, *etc.*, were measured by DLS measurement, UV-Visible spectrophotometer, fluorescence spectrometer, femtosecond laser, CCK-8 kit, respectively. The nucleolus-targeting capability of C-dots was investigated using fluorescence imaging. The HeLa cells were incubated with C-dots and irradiated with a femtosecond laser before cell viability was examined using Calcein-AM/PI staining and fluorescence imaging.

Results and Discussions The microwave heating method selects citric acid and ethylenediamine as raw materials to synthesize the C-dots. The synthesized C-dots were studied using dynamic light scattering measurement, and the average size of the C-dots was approximately 1 nm [Fig. 2(a)]. The C-dots absorbed light in various wavelengths from 300 to 700 nm, with the main absorption peak at 360 nm and a shoulder peak at 450 nm [Fig. 2(b)]. The C-dots exhibited excitation-dependent emission [Fig. 2(c)] and significant two-photon fluorescence when exposed to femtosecond laser irradiation [Fig. 2(d)]. The ROS-generation capability of the C-dots in aqueous solutions was investigated using ABDA as the ROS indicator under white light irradiation (400–700 nm, 100 mW/cm^2). The ABDA was almost decomposed after 10 min illumination [Fig. 2(e)], indicating the ROS-generation capability of the C-dots. The long-term stability and photostability of the C-dots were characterized by measuring the absorption spectra at different time points [Fig. 2(f)] and after continuous irradiation [Fig. 2(g)], respectively. The experimental results showed that the C-dots had good long-term stability and photostability. CCK-8 kits were used to evaluate the biocompatibility of the C-dots before undergoing *in vitro* photodynamic therapy. For 24 and 48 h, no significant difference existed between control cells and cells treated with the C-dots in the mass concentration range of 250–750 g/mL, indicating the excellent biocompatibility of the C-dots. The C-dots were treated with HeLa cells to investigate their intracellular position, followed by fluorescence imaging. The fluorescence signal of the C-dots was observed in some round areas, i.e., nucleoli. HeLa cells were co-stained with the C-dots and one commercial nucleolus imaging probe, SYTO RNASelect, to demonstrate the C-dots'

nucleolus-targeting capacity. Figure 3 showed the fluorescence of the C-dots completely overlapped with that of SYTO RNASelect, confirming that the C-dots could specifically stain the nucleolus. HeLa cells were cultured with/without the C-dots (500 g/mL) for 3 h before being exposed to femtosecond laser irradiation to study the two-photon PDT efficiency of the C-dots (740 nm, 28 mW). The treated cells were incubated for 4 h following the irradiation and stained with Calcein-AM and PI. Figure 4 showed that more cells were PI-positive with an increment of irradiation time. When the irradiation time reached 45 s, almost all cells were necrotic, suggesting the excellent cancer cell ablation potential of nucleolus-targeted two-photon photodynamic treatment. The identical irradiation did not result in necrosis in the absence of the C-dots, indicating that laser irradiation had no effect.

Conclusions We designed and synthesized novel C-dots with intrinsic nucleolus-targeting and ROS-generation capabilities. The nucleolus-targeted two-photon PDT exhibits outstanding cancer cell ablation efficiency at a low dose of the C-dots and light irradiation because the C-dots generated ROS is positioned within the nucleolus, which is an efficient cancer therapy site. Additionally, the developed C-dots possess some unique advantages, including ultrasmall size, long-term stability, and excellent biocompatibility, making them promising for practical two-photon PDT applications.

Key words medical optics; photodynamic therapy; two-photon absorption; nucleolus targeting; carbon dots